



Design, synthesis and biological evaluation of a novel tubulin inhibitor SKLB0565 targeting the colchicine binding site

Xi Hu¹, Lu Li¹, Qiangsheng Zhang, Qianqian Wang, Zhanzhan Feng, Ying Xu, Yong Xia*, Luoting Yu*

State Key Laboratory of Biotherapy and Cancer Center, West China Hospital, West China Medical School, Sichuan University, and Collaborative Innovation Center for Biotherapy, 17#3rd Section, Ren Min South Road, Chengdu 610041, China

ARTICLE INFO

Keywords:

Tubulin polymerization inhibitors
Colchicine binding site
Anti-proliferative
Colorectal carcinoma

ABSTRACT

A series of 3-(((9H-purin-6-yl) amino) methyl) pyridin-2(1H)-one derivatives were designed, synthesized and confirmed as tubulin polymerization inhibitors. All compounds were evaluated for their anti-proliferative activities on three colorectal carcinoma (CRC) cell lines. Among these compounds, SKLB0565 displayed noteworthy potency against eight CRC cell lines with IC₅₀ values ranging from 0.012 μM and 0.081 μM. Besides, SKLB0565 inhibited tubulin polymerization, caused G2/M phase cell cycle arrest, depolarized mitochondria and induced cell apoptosis in CRC cells. Furthermore, SKLB0565 suppressed cell migration and disrupted the capillary tube formation of human umbilical vein endothelial cells (HUVECs). Our data clarified that SKLB0565 is a promising anti-tubulin agent for CRC therapy which is worthy of further evaluation.

1. Introduction

Microtubules, which are widely expressed in eukaryotic cells, are tubular polymers formed by polymerization of α - and β -tubulin with molecular weights of about 55 kDa [1,2]. They are main components of the cytoskeleton and play pivotal roles in numerous cellular activities, such as maintaining cell morphology and transporting intracellular material, especially during cell division and proliferation [3–5]. Microtubules maintain the balance of dynamic polymerization and depolymerization in normal cells. However, the irreversible destruction of microtubule dynamic polymerization balance is often closely related to the progression of cancer [6]. Therefore, microtubules have been considered to be a promising target for cancer chemotherapy [7,8].

Lots of tubulin inhibitors have been successfully used in the clinic and many more are under preclinical and clinic evaluation, such as paclitaxel [9], colchicine [10], combretastatin A-4 (CA-4) [11,12] and SAMRT [13] (Fig. 1A). Based on the analysis of the chemical structure of reported microtubule inhibitors, our research interest focuses on novel microtubule inhibitors containing concise double-ring core structure, such as MPC-6827 [14], Compound 30HCl [15], Compound 60 [16], Myoseverin [17]

and BNC105 [18]. We designed and synthesized a series of 3-(((9H-purin-6-yl)amino)methyl-4,6-dimethylpyridin-2(1H)-one derivatives using a bioelectronic isosteric strategy in our previous study. Biological evaluation indicated that this class of compounds were antimetabolic agents and exerted their anticancer action through inhibition of tubulin polymerization. In particular, one of the compounds SKLB0533 showed strong anti-proliferative effects in CRC cells. Furthermore, SKLB0533 showed excellent target selectivity and exhibited no inhibitory activities against other potential targets, including 420 kinases and EZH2 [19]. All of these indicated that this series of compounds deserve further study to obtain more potent compounds, as well as to explore their structure activity relationships (SARs) more perfectly.

In this study, we focus on the effects of different pyridine-2(1H)-one substitutions on their anti-proliferative activities and aim to find more potent compounds targeting the colchicine binding site to complement our previous research. We designed and synthesized a series of 3-(((9H-purin-6-yl) amino) methyl) pyridin-2(1H)-one derivatives, analyzed the SARs of different pyridine-2(1H)-one substitutions and evaluated their anti-CRC activities of this class of compounds (Fig. 1B).

* Corresponding authors at: Lab of Medicinal Chemistry, State Key Laboratory of Biotherapy and Cancer Center, West China Hospital, Sichuan University and Collaborative Innovation Center for Biotherapy, 17#3rd Section, Ren Min South Road, Chengdu 610041, China.

E-mail addresses: scuxiyong@163.com (Y. Xia), yuluot@scu.edu.cn (L. Yu).

¹ These authors contribute equally to this work.

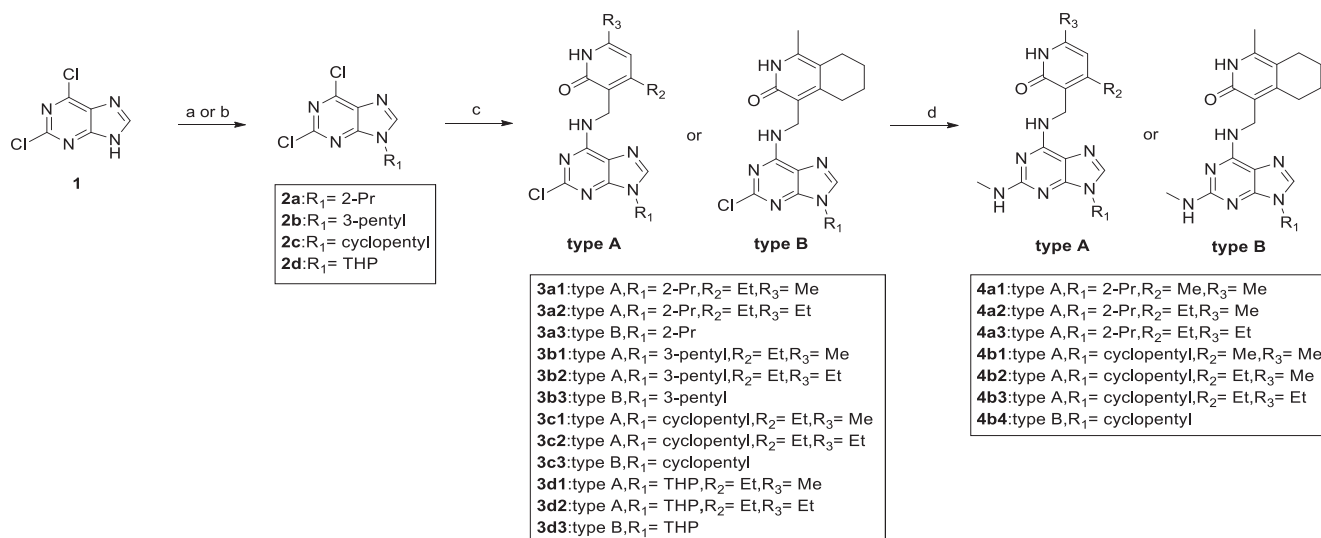
<https://doi.org/10.1016/j.bioorg.2020.103695>

Received 28 January 2020; Received in revised form 21 February 2020; Accepted 22 February 2020

Available online 24 February 2020

0045-2068/ © 2020 The Authors. Published by Elsevier Inc. This is an open access article under the CC BY-NC-ND license

(<http://creativecommons.org/licenses/by-nc-nd/4.0/>).



Scheme 1. Synthesis of target compounds. (a) Halogenated alkane, K₂CO₃, anhydrous DMSO, 15 °C, overnight. (b) 3,4-Dihydro-2H-pyran, *p*-TsOH, DCM, r.t., 8h. (c) 3-(aminomethyl)-4-ethyl-6-methylpyridin-2(1H)-one, 3-(aminomethyl)-4,6-diethylpyridin-2(1H)-one or 4-(aminomethyl)-1-methyl-5,6,7,8-tetrahydroisoquinolin-3(2H)-one, EtOH, 80 °C, 6 h. (d) Aqueous methylamine, sealed tube, 110 °C, 5 h.

2.2. Structure-activity relationships

To better understand the SARs of the newly synthesized compounds, the IC₅₀ values were obtained by MTT cytotoxicity assay. According to previous studies, SKLB0533 exhibited notable anti-proliferative effects on CRC cells. Therefore, we continued to evaluate the anti-proliferative activities of these compounds against three CRC cell lines CT26, SW20 and HCT116, CA-4 and SKLB0533 served as the positive references (Table 1).

In general, when the N9-position of purine ring was substituted by 2-Pr, 3-pentyl, cyclopentyl or THP, all of the compounds exhibited good anti-proliferative activities. Incorporation of a cyclopentyl group at 9-position of purine ring (**3c1–3c3**), demonstrated improved cellular activities compared to 3-pentyl and THP substituents (**3b1–3b3**,

Table 1
Anti-proliferative activities of the compounds against three CRC cell lines.^a

Cpd.	IC ₅₀ values (μM) ^b		
	CT26	SW620	HCT116
3a1	0.101 ± 0.011	0.072 ± 0.001	< 0.002
3a2	0.022 ± 0.011	0.009 ± 0.002	0.058 ± 0.003
3a3	> 5	1.350 ± 0.054	0.038 ± 0.002
3b1	0.023 ± 0.003	0.409 ± 0.058	0.077 ± 0.003
3b2	0.021 ± 0.006	0.244 ± 0.001	0.104 ± 0.007
3b3	0.086 ± 0.021	1.908 ± 0.164	3.232 ± 0.022
3c1	0.049 ± 0.002	0.031 ± 0.004	0.510 ± 0.390
3c2 (SKLB0565)	0.057 ± 0.007	0.040 ± 0.011	0.021 ± 0.003
3c3	1.255 ± 0.193	0.312 ± 0.010	0.839 ± 0.021
3d1	0.088 ± 0.007	0.097 ± 0.018	2.761 ± 0.197
3d2	0.064 ± 0.019	0.043 ± 0.007	0.039 ± 0.000
3d3	4.772 ± 0.158	0.958 ± 0.026	2.250 ± 0.243
4a1	2.790 ± 0.72	0.176 ± 0.053	0.142 ± 0.013
4a2	0.619 ± 0.162	0.103 ± 0.006	0.099 ± 0.018
4a3	> 5	0.317 ± 0.037	0.479 ± 0.088
4b1	1.498 ± 0.023	0.214 ± 0.017	0.138 ± 0.029
4b2	0.616 ± 0.115	0.120 ± 0.011	0.043 ± 0.003
4b3	0.192 ± 0.064	0.078 ± 0.011	0.019 ± 0.007
4b4	> 5	1.133 ± 0.057	1.329 ± 0.077
SKLB0533	0.052 ± 0.012	0.062 ± 0.001	0.072 ± 0.003
CA-4	0.114 ± 0.013	0.029 ± 0.006	0.128 ± 0.005

^a Cell lines were treated with different concentrations of compounds for 72 h.

^b IC₅₀ values are indicated as the mean ± SEM of at least two independent experiments.

3d1–3d3). In our previous studies, the steric effect of substituents on the C2-position of purine ring was crucial to the anti-proliferative activities [21]. To exclude the possibilities that the anti-proliferative effects were caused by the departure of chlorine atom, the chlorine atom at 2-position of purine in **3c2** was replaced with aminomethyl substitution to obtain **4b3**, which maintained the anti-proliferative activity, suggesting that **3c2** might not exert anti-proliferative efficacy through the departure of chlorine atom.

Then we focused on the effects of different pyridin-2(1H)-one substitutions at the 9-position of purine ring on anti-proliferative activities. As shown in Table 1, the anti-proliferative activities of the synthesized compounds with different pyridin-2(1H)-one substitutions increased in the following order: compounds **3a2**, **3b2**, **3c2**, **3d2**, **4a3** and **4b3** (4,6-diethylpyridin-2(1H)-one) > compounds **3a1**, **3b1**, **3c1**, **3d1**, **4a2** and **4b2** (4-ethyl-6-methylpyridin-2(1H)-one) > compounds **3a3**, **3b3**, **3c3**, **3d3** and **4b4** (1-methyl-5,6,7,8-tetrahydroisoquinolin-3(2H)-one). When comparing compound **3c3** with SKLB0533, compound **4a3** with compound **4a1** and compound **4b3** with compound **4b1**, the data indicated that the 4,6-diethylpyridin-2(1H)-one substituent might interact more strongly with the amino acids surrounding the binding pocket, which was confirmed in subsequent molecular modeling studies.

Most of the synthesized compounds inhibited the growth of the tested CRC cell lines, with IC₅₀ values less than 1 μM. Notably, compound **3c2** (SKLB0565) exhibited the most potent anti-proliferative activity among all compounds, with IC₅₀ values ranging between 0.021 and 0.057 μM. Moreover, SKLB0565 was more active against the tested CRC cell lines than SKLB0533 in our study. Therefore, SKLB0565 was selected for further pharmacodynamic study.

2.3. Effects of SKLB0565 on tubulin polymerization and microtubule

The effects of SKLB0565 on tubulin polymerization were determined by a fluorescence-based tubulin polymerization kit in cell free condition, and paclitaxel and CA-4 were used as positive controls. As shown in Fig. 2A, paclitaxel exhibited significant promotion of tubulin polymerization, while compound SKLB0565, which was similar to CA-4, displayed a concentration-dependent inhibition of tubulin polymerization. These results indicated that SKLB0565 was able to effectively inhibit the polymerization of tubulin *in vitro*.

Since inhibition of tubulin polymerization would cause damage of microtubule networks and cytoskeleton [22], we subsequently

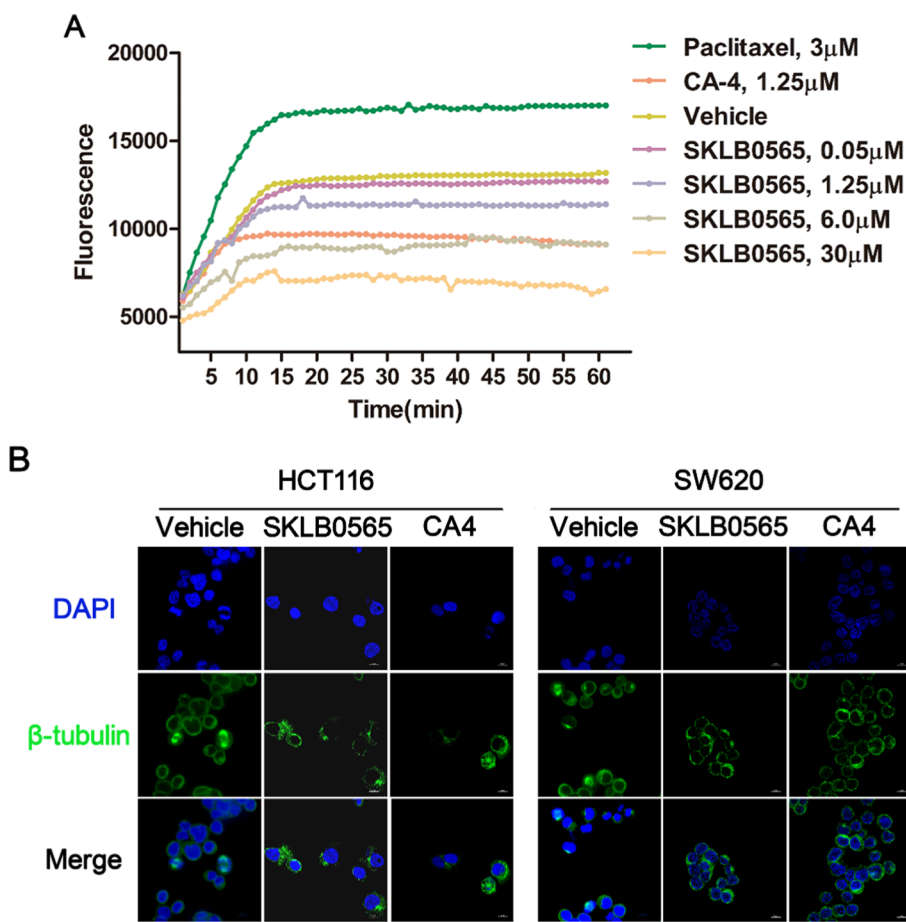


Fig. 2. Effects of SKLB0565 on tubulin polymerization (A) and microtubule networks (B) *in vitro*. (A) 2 mg/mL purified tubulin protein in reaction buffer was incubated at 37 °C in the presence of 0.1% DMSO, SKLB0565 (0.05, 1.25, 6.0, 30 μ M), Paclitaxel (3 μ M) or CA-4 (1.25 μ M). Polymerizations were followed by an increase in fluorescence excitation at 355 nm and fluorescence emission at 460 nm over a 60 min period at 37 °C. (B) Both cells were treated with 0.1% DMSO, SKLB0565 (50 nM) or CA-4 (50 nM) for 18 h. Microtubule networks were visualized with an anti- β -tubulin-FITC antibody (green), and the cell nucleus were visualized with DAPI (blue). (For interpretation of the references to colour in this figure legend, the reader is referred to the web version of this article.)

performed the immunofluorescence assays to investigate the effects of compound SKLB0565 on microtubule networks in HCT116 and SW620 cells. As shown in Fig. 2B, the microtubule networks in the cells exhibited a normal filamentous arrangement without drug treatment. However, when treated with SKLB0565 or CA-4 at the concentration of 50 nM for 18 h, the microtubule organization in the cytosol was disrupted and shrank to the nucleus. These results indicated that SKLB0565 could cause the disintegration of intracellular microtubule networks, which would potentially lead to cell cycle disorder [23].

2.4. Molecular docking

The binding mode and type of interaction between SKLB0565 and tubulin (PDB code: 4O2B) were investigated by molecular docking. As shown in Fig. 3A, SKLB0565 could well bind to colchicine binding site of tubulin, and the binding mode was similar to that of colchicine. There were hydrogen bonds between the ketone of pyridin-2(1H)-one fragment and the NH of Asp β 251, the N7 of purine ring and the NH of Asn β 258. The NH of pyridin-2(1H)-one fragment of SKLB0565 could form a hydrogen interaction with the carbonyl of Asp β 251, but SKLB0533 did not form the hydrogen interaction (Fig. 3B). We speculated that the 4, 6-diethyl group of pyridin-2(1H)-one caused a slight change in the spatial conformation of pyridine, which could better adapt to the binding pocket. Besides the hydrogen interactions, there were some hydrophobic interactions with the surrounding residues.

2.5. *In vitro* anti-proliferative activities of SKLB0565

The growth inhibitory activities of SKLB0565 were further evaluated by MTT assay against some other CRC cell lines. The data in Table 2 showed that SKLB0565 dramatically inhibited the viabilities of

the CRC cells after 72 h of treatment, and the IC₅₀ values were all below 100 nM. Therefore, we chose HCT116 and SW620 to further study the efficacy of SKLB0565 against CRC cells.

As shown in Fig. 4A, after treatment with different concentrations of SKLB0565 for 24, 48 or 72 h, the viabilities of both HCT116 and SW620 cells were inhibited in different degrees, indicating that SKLB0565 suppressed cell proliferation in a time- and concentration-dependent manner. Colony formation assay was also used to assess the sensitivity of CRC cells to SKLB0565 over a relatively long exposure time (14 days). As shown in Fig. 4B, both the size and number of clones in HCT116 and SW620 cells were decreased at low concentration of SKLB0565.

2.6. SKLB0565 treatment caused G2/M cell cycle arrest of CRC cells

Since most microtubule polymerization inhibitors could disrupt cell mitosis and exert the G2/M arrest on cell cycle [24,25], the effects of SKLB0565 on cell cycle progression in HCT116 and SW620 cells were examined by flow cytometry (FCM) analysis after propidium iodide (PI) staining. As shown in Fig. 5A, the proportion of cells in G2/M phase increased with the increase of SKLB0565, suggesting that SKLB0565 could cause G2/M phase cell cycle arrest in a dose-dependent manner.

The alterations of protein expression involved in G2/M phase regulations were detected to elucidate how SKLB0565 caused cell cycle arrest. As indicated in Fig. 5B, SKLB0565 increased the expression of CyclinB1 and CDK1, and decreased that of pCDK1 (Y15). Meanwhile, the expression of cdc25c, which catalyzes the dephosphorylation of pCDK1 (Y15), was upregulated. Our data indicated that SKLB0565 caused the increase activities of CyclinB1-CDK1 complex in CRC cells and might lead to cell cycle arrest through this mechanism.

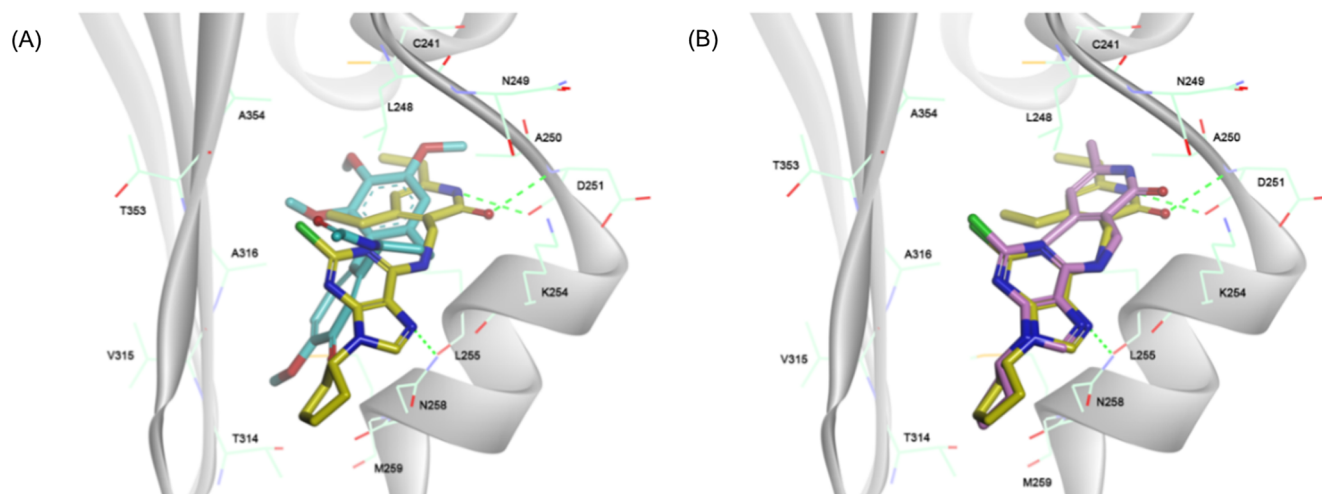


Fig. 3. Predicted binding mode of SKLB0565 (yellow stick) with tubulin (PDB code: 4O2B) and overlapping with colchicine (blue stick) (A) and SKLB0533 (carminc stick) (B). Hydrogen bonds are shown as green dashed lines. (For interpretation of the references to colour in this figure legend, the reader is referred to the web version of this article.)

Table 2
Effects of SKLB0565 on CRC cell viabilities^a.

Cell lines	Cell type	IC ₅₀ (μM) ^b
HCT116	Colorectal carcinoma	0.012 ± 0.003
SW620	Colorectal carcinoma	0.028 ± 0.001
SW480	Colorectal carcinoma	0.081 ± 0.004
SW48	Colorectal carcinoma	0.015 ± 0.003
DLD-1	Colorectal carcinoma	0.074 ± 0.008
HCT15	Colorectal carcinoma	0.029 ± 0.001
HT29	Colorectal carcinoma	0.029 ± 0.001
CT26	Colorectal carcinoma	0.052 ± 0.001

^a Cell lines were treated with different concentrations of SKLB0565 for 72 h.

^b IC₅₀ values are indicated as the mean ± SEM of at least two independent experiments.

2.7. SKLB0565 treatment caused apoptosis of CRC cells

To analyze the mode of cell death induced by SKLB0565, FCM analysis was performed after FITC-Annexin-V/PI staining. PI, could enter dead cells and intercalate in DNA, and Annexin-V, could bind to phosphatidyl serine of valgus at the initial stage of apoptosis [26]. It can be observed from Fig. 6A that the total percentages of early and late apoptotic cells were significantly elevated with the increasing concentration of SKLB0565. The data showed that 100 nM of SKLB0565 caused apoptosis rates of 43.27% and 31.23% after 48 h treatment in HCT116 and SW620 cells, respectively. Whereas the apoptosis rates of untreated cells were only 3.39% and 8.60%. The morphological changes of SW620 cells' nuclei after SKLB0565 treatment were analyzed through Hoechst 33342 staining [27]. As seen in Fig. 6B, the apoptotic cells showed bright blue fluorescent and condensed nuclei, which were only seen in the SKLB0565 treated cells. These results showed that SKLB0565 significantly induced CRC cell apoptosis in a dose-dependent manner.

2.8. Effects of SKLB0565 on the mitochondrial membrane potential ($\Delta\Psi_m$)

In order to gain insight into the underlying mechanism of cell apoptosis induced by SKLB0565, several apoptosis-related proteins were detected by western blot. As shown in Fig. 7A, the expression of cleaved caspase-9, which plays an important role in mitochondrial-mediated intrinsic apoptosis pathway [28,29], was up-regulated after

treatment with SKLB0565 for 48 h, indicating the activation of caspase-9. This phenomenon indicated that the mitochondria-mediated intrinsic apoptotic pathway might be involved in SKLB0565 induced apoptosis. The disruption of $\Delta\Psi_m$ is an important event in the mitochondrial apoptosis pathway [29,30]. Then, a mitochondria-specific and voltage-dependent dye Rhodamine 123 (Rh123) was used to detect the $\Delta\Psi_m$ changes in both cell lines. The results in Fig. 7B showed that $\Delta\Psi_m$ decreased after treatment with the increasing concentration of SKLB0565, indicating that SKLB0565 induced apoptosis probably via the intrinsic mitochondrial apoptosis pathway. Furthermore, the expression of PARP, a downstream cleavage substrate of caspase-3, and the expression of Bcl-2 and Bax, two Bcl-2 family proteins, which are involved in the regulation of mitochondrial membrane permeability [31,32], were also detected (Fig. 7A). After exposure to SKLB0565 for 48 h, the level of cleaved PARP increased significantly. Additionally, the expression of Bcl-2 was down-regulated and that of Bax was up-regulated after SKLB0565 treatment for 48 h. All of these results suggested that the endogenous mitochondrial mediated apoptosis pathway was involved in SKLB0565 induced apoptosis.

2.9. In vitro anti-vascular activity of SKLB0565

HUVECs were used to investigate the anti-vascular activity of SKLB0565. Because microtubule networks control some cell migration events [5], the inhibition of SKLB0565 on HUVECs migration was detected by wound healing assay. As we can see in Fig. 8A, the scratch in the SKLB0565 treated cell cultures healed slower than that in the untreated cell culture.

Colchicine site binding agents could block the vasculogenesis within solid tumors and a number of them have been in anticancer clinical investigations [33]. Thus, we carried out capillary tube formation assay to evaluate the anti-vascular activity of SKLB0565. HUVECs could form capillary-like tubes with multicentric junctions after being seeded on matrigel. As shown in Fig. 8B, after exposure to SKLB0565 at doses of 50 and 100 nM for 6 h, the capillary-like tubes were damaged in different levels, suggesting that SKLB0565 effectively inhibited the tube formation of HUVECs. These results confirmed that SKLB0565 was able to inhibit vasculogenesis *in vitro*.

3. Conclusions

In the present study, we have designed, synthesized and evaluated the anti-CRC efficacies of a series of novel 3-(((9H-purin-6-yl) amino)

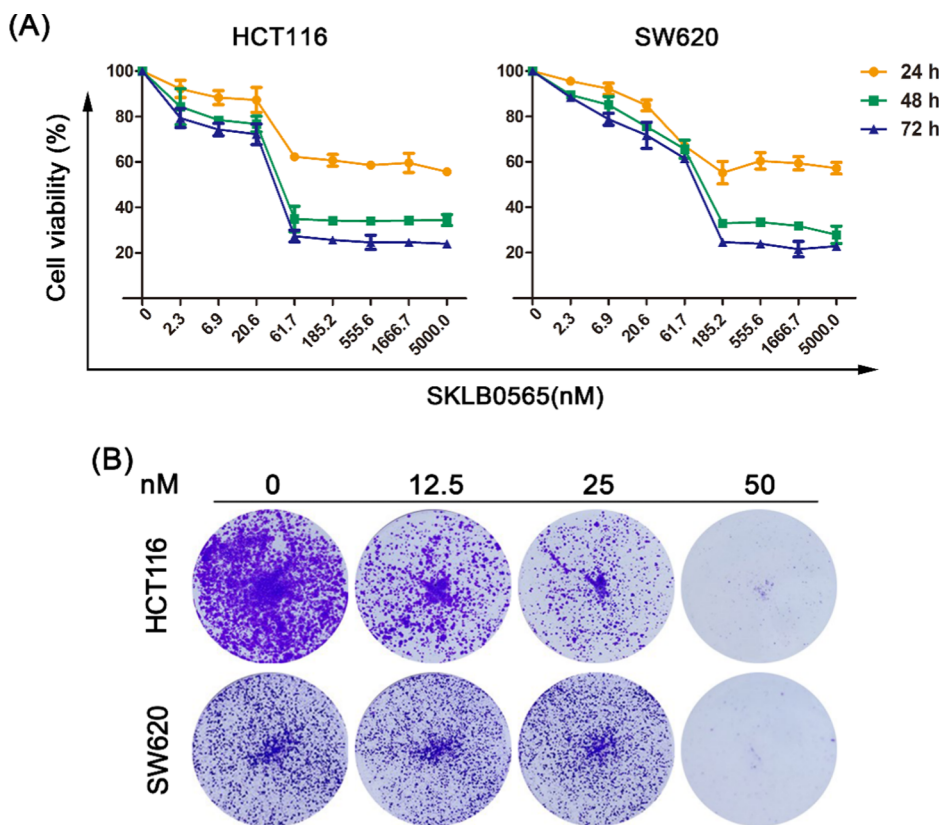


Fig. 4. Anti-proliferative activities of SKLB0565 on HCT116 and SW620 cells measured by MTT and colony formation assays. (A) The growth inhibitory activities of SKLB0565 against HCT116 and SW620 cells at different time points. (B) Representative colony formation images of HCT116 and SW620 cells after exposure to SKLB0565 for 14 days.

methyl) pyridin-2(1H)-one derivatives based on the previously reported SKLB0533. Anti-proliferative screening of these newly synthesized compounds showed that the representative compound SKLB0565 exhibited noteworthy nanomolar potency against a series of CRC cell lines. It showed inhibitory activity on tubulin polymerization and the ability to bind to colchicine site. Further mechanism studies illustrated that SKLB0565 caused abnormal cellular microtubules and G2/M phase cell cycle arrest, depolarized mitochondria, and induced cell apoptosis in CRC cell lines. Additionally, wound healing and capillary tube formation assays showed that SKLB0565 was a potent vascular disrupting agent. Taken together, SKLB0565 showed impressing anti-CRC activities *in vitro* and is a potential anti-tubulin agent for CRC treatment.

4. Experimental

4.1. Chemistry

Unless otherwise noted, all materials were obtained from commercial suppliers and used without further purification. Melting point (mp) was measured on hot-stage microscope (Shanghai Precision Scientific Instruments Co., Ltd, X-4). The ^1H and ^{13}C NMR spectra were recorded on a Bruker Avance 400 spectrometer at 25 °C using DMSO- d_6 , CD $_3$ OD or CDCl $_3$ as the solvent. Chemical shifts (δ) are reported in ppm relative to Me $_4$ Si (internal standard), coupling constants (J) are reported in hertz, and peak multiplicity are reported as s (singlet), d (doublet), t (triplet), q (quartet), m (multiplet), or br s (broad singlet). High resolution mass analysis was performed on a Waters Q-TOF Premier mass spectrometer with electron spray ionization (ESI). Thin layer chromatography (TLC) was performed on 0.20 mm silica gel F-254 plates (Qingdao Haiyang Chemical, China). Visualization of TLC was accomplished with UV light and/or aqueous potassium permanganate or I $_2$ in a silica gel. Column chromatography was performed using silica gel 60 of 300–400 mesh (Qingdao Haiyang Chemical, China).

4.1.1. The representative procedure for the preparation of 2,6-dichloro-9H-purine derivatives (2a–2c)

2,6-dichloro-9-isopropyl-9H-purine (2a). 2,6-dichloro-9H-purine (1.0 g, 5.29 mmol), and potassium carbonate (K $_2$ CO $_3$) (2.193 g, 15.87 mmol) were dissolved in 20 mL anhydrous DMSO. Iodopropane (2.64 mL, 26.45 mmol) was added dropwise at 15 °C. The reaction mixture was stirred at 15 °C overnight. Upon completion of the reaction, the reaction solution was poured into ice water, and a white solid precipitated. The solution was filtered and dried under a vacuum to give 1.1 g of light yellow solid. Yield: 90.02%. ^1H NMR (400 MHz, DMSO- d_6) δ 8.86 (s, 1H), 4.83 (p, J = 6.8 Hz, 1H), 1.56 (d, J = 6.8 Hz, 6H).

2,6-dichloro-9-(pentan-3-yl)-9H-purine (2b). White solid, yield: 81.75%. ^1H NMR (400 MHz, DMSO- d_6) δ 8.85 (s, 1H), 4.38 (tt, J = 8.8, 5.6 Hz, 1H), 2.10–1.85 (m, 4H), 0.72 (t, J = 7.4 Hz, 6H).

2,6-dichloro-9-cyclopentyl-9H-purine (2c). White solid, yield: 58.82%. ^1H NMR (400 MHz, DMSO- d_6) δ 8.82 (s, 1H), 4.93 (p, J = 7.4 Hz, 1H), 2.20 (dq, J = 12.7, 6.7 Hz, 2H), 2.02 (dq, J = 13.6, 7.1 Hz, 2H), 1.89 (m, 2H), 1.77–1.64 (m, 2H).

4.1.2. Synthesis of 2,6-dichloro-9-(tetrahydro-2H-pyran-2-yl)-9H-purine (2d)

2,6-dichloro-9H-purine (4.62 g, 24.03 mmol), 3,4-dihydropyran (4.38 g, 48.06 mmol) and *p*-toluenesulfonic acid (0.27 g, 1.44 mmol) were added to a 250 mL round bottom flask. DCM was used as the solvent, and the solution was reacted at room temperature for 8 h. After the reaction was completed, the reaction solution was washed with water. The organic phase was collected and dried under a vacuum to give crude the product. The crude product was then purified by silica gel column chromatography to afford 6.5 g of the target compounds as white solid with yield 99.01%. ^1H NMR (400 MHz, DMSO- d_6) δ 8.95 (s, 1H), 5.74 (dd, J = 10.8, 2.3 Hz, 1H), 4.10–3.93 (m, 1H), 3.78–3.66 (m, 1H), 2.31–2.19 (m, 1H), 2.07–1.88 (m, 2H), 1.82–1.71 (m, 1H), 1.60 (p, J = 5.9, 4.9 Hz, 2H).

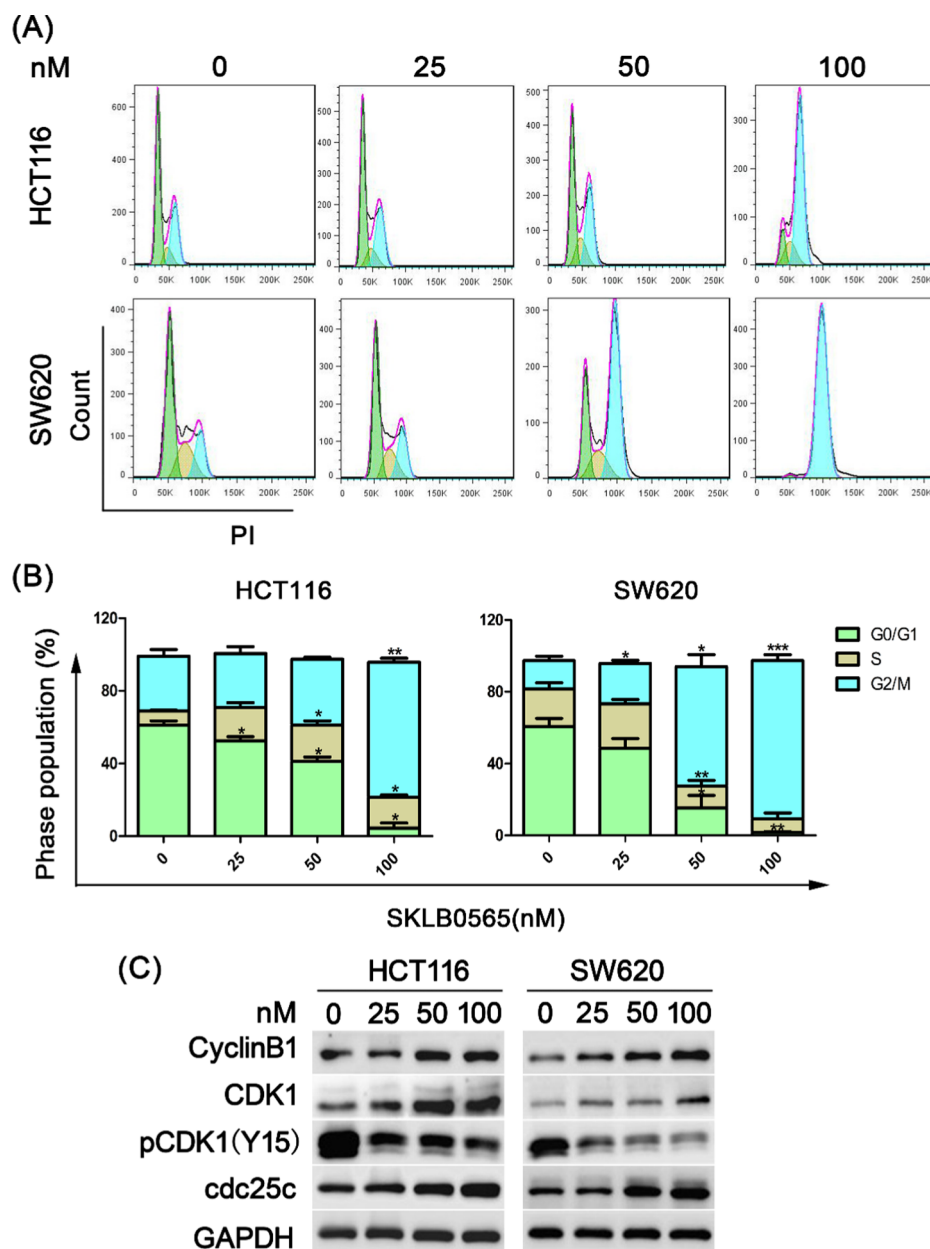


Fig. 5. SKLB0565 caused G2/M phase cell cycle arrest in HCT116 and SW620 cells. (A) Cells were treated with increasing doses of SKLB0565 for 24 h and then analyzed by FCM. (B) Quantified histograms display the effects of SKLB0565 on HCT116 and SW620 cell cycle progression. Data are expressed as means \pm SD for 3 independent experiments, * $p < 0.05$, ** $p < 0.01$, *** $p < 0.001$, compared with the vehicle control group by *t*-test. (C) After treatment with indicated concentrations of SKLB0565 for 24 h, the cells were harvested and lysed for detection of several key cell cycle regulating proteins.

4.1.3. The representative procedure for the preparation of 3-(((2-chloro-9-substituted-9H-purin-6-yl)amino)methyl)-pyridin-2(1H)-one derivatives (3a1–3d3)

3-(((2-chloro-9-isopropyl-9H-purin-6-yl)amino)methyl)-4-ethyl-6-methylpyridin-2(1H)-one (**3a1**), 2,6-dichloro-9-isopropyl-9H-purine (**2a**) (300.00 mg, 1.30 mmol), 3-(aminomethyl)-4-ethyl-6-methylpyridin-2(1H)-one (258.95 mg, 1.56 mmol), obtained following the reference procedure [21]), and triethylamine (0.90 mL, 6.50 mmol) were added to ethanol (10 mL), and the reaction solution was reacted under reflux at 80 °C for 5 h. After completion (monitored by TLC), the reaction mixture was removed under vacuum and extracted with DCM. The organic layers were dried over anhydrous sodium sulphate, filtered and concentrated under reduced pressure. The crude product was purified by silica gel column chromatography to afford target compounds as white solid with yield 91.23%, mp 215–217 °C. ^1H NMR (400 MHz, DMSO- d_6) δ 11.56 (s, 1H), 8.24 (s, 1H), 7.69 (t, $J = 5.5$ Hz,

1H), 5.92 (s, 1H), 4.71–4.62 (m, 1H), 4.49 (d, $J = 5.2$ Hz, 2H), 2.63 (q, $J = 7.3$ Hz, 2H), 2.13 (s, 3H), 1.49 (d, $J = 6.8$ Hz, 6H), 1.11 (t, $J = 7.6$ Hz, 3H). ^{13}C NMR (101 MHz, DMSO- d_6) δ 164.01, 155.01, 153.13, 149.73, 143.84, 139.90, 121.03, 118.96, 106.36, 47.22, 36.63, 25.90, 22.55 (2C), 18.78, 14.90. HRMS (ESI): calcd. for $\text{C}_{17}\text{H}_{21}\text{ClN}_6\text{NaO}$ [$\text{M} + \text{Na}$] $^+$: 383.1363 found: 383.1355.

3-(((2-chloro-9-isopropyl-9H-purin-6-yl)amino)methyl)-4,6-diethylpyridin-2(1H)-one (**3a1**). White solid, yield: 87.32%, mp 187–189 °C. ^1H NMR (400 MHz, DMSO- d_6) δ 11.55 (s, 1H), 8.24 (s, 1H), 7.69 (t, $J = 7.9$ Hz, 1H), 5.94 (d, $J = 4.4$ Hz, 1H), 4.71–4.62 (m, 1H), 4.49 (d, $J = 5.5$ Hz, 2H), 2.64 (q, $J = 7.7$ Hz, 2H), 2.43 (q, $J = 7.7$ Hz, 2H), 1.48 (t, $J = 6.9$ Hz, 6H), 1.12 (t, $J = 6.8, 6.1$ Hz, 6H). ^{13}C NMR (101 MHz, Chloroform- d) δ 165.72, 156.34, 154.99, 154.11, 149.70, 149.27, 137.16, 121.27, 119.11, 106.18, 46.75, 36.56, 26.35, 26.20, 22.79 (2C), 14.81, 12.69. HRMS (ESI): calcd. for $\text{C}_{18}\text{H}_{23}\text{ClN}_6\text{NaO}$ [$\text{M} + \text{Na}$] $^+$: 397.1520 found: 397.1513.

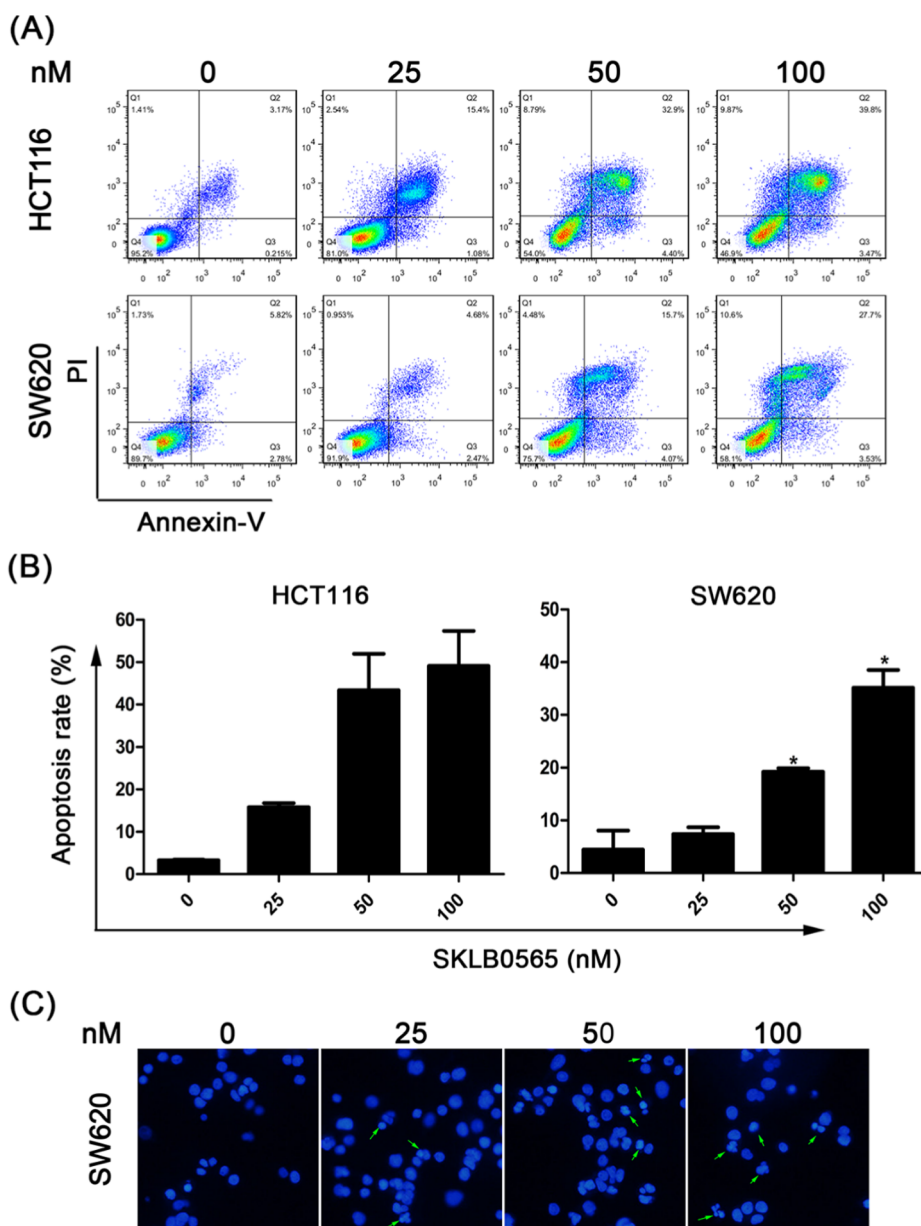


Fig. 6. SKLB0565 induced apoptosis in HCT116 and SW620 cells. (A) The cells were treated with increasing doses of SKLB0565 for 48 h and analyzed by FCM after Annexin V/PI staining. (B) Quantified histograms display the proportions of apoptotic cells. Data are expressed as means \pm SD for 3 independent experiments, * $p < 0.05$, compared with the vehicle control group by t -test. (C) After treatment with indicated concentrations of SKLB0565 for 48 h, the cells were stained with Hoechst 33422 (10 μ g/mL) and visualized by fluorescence microscopy.

4-(((2-chloro-9-isopropyl-9H-purin-6-yl)amino)methyl)-1-methyl-5,6,7,8-tetrahydro isoquinolin-3(2H)-one (**3a3**). White solid, yield: 93.10%, mp 284–286 °C. ¹H NMR (400 MHz, DMSO-*d*₆) δ 11.54 (s, 1H), 8.23 (s, 1H), 7.79 (t, $J = 5.2$ Hz, 1H), 4.76–4.53 (m, 1H), 4.46 (d, $J = 5.1$ Hz, 2H), 2.87 (s, 2H), 2.38 (s, 2H), 2.10 (s, 3H), 1.64 (t, $J = 5.2$ Hz, 5H), 1.49 (d, $J = 6.8$ Hz, 6H). ¹³C NMR (101 MHz, DMSO-*d*₆) δ 162.16, 155.14, 153.09, 150.26, 149.71, 141.05, 139.82, 120.97, 118.96, 112.27, 47.21, 36.83, 27.02, 24.66, 22.55, 22.44, 16.44. HRMS (ESI): calcd. for C₁₉H₂₃ClN₆NaO [M + Na]⁺: 409.1520 found: 405.1519.

3-(((2-chloro-9-(pentan-3-yl)-9H-purin-6-yl)amino)methyl)-4-ethyl-6-methylpyridin-2(1H)-one (**3b1**). White solid, yield: 89.38%, mp 197–199 °C. ¹H NMR (400 MHz, DMSO-*d*₆) δ 11.56 (s, 1H), 8.21 (s, 1H), 7.72 (t, $J = 5.5$ Hz, 1H), 6.04–5.75 (m, 1H), 4.49 (d, $J = 5.0$ Hz, 2H), 4.25–4.09 (m, 1H), 2.64 (q, $J = 7.6$ Hz, 2H), 2.13 (s, 3H), 1.99–1.70 (m, 4H), 1.12 (t, $J = 7.6$ Hz, 3H), 0.69 (t, $J = 7.3$ Hz, 6H). ¹³C NMR

(101 MHz, Chloroform-*d*) δ 165.74, 156.38, 154.91, 154.14, 150.49, 143.77, 138.24, 121.10, 118.89, 107.98, 58.81, 36.48, 27.76 (2C), 26.22, 18.95, 14.75, 10.48 (2C). HRMS (ESI): calcd. for C₁₉H₂₅ClN₆NaO [M + Na]⁺: 411.1676 found: 411.1673.

3-(((2-chloro-9-(pentan-3-yl)-9H-purin-6-yl)amino)methyl)-4,6-diethylpyridin-2(1H)-one (**3b2**). White solid, yield: 86.58%, mp 146–148 °C. ¹H NMR (400 MHz, DMSO-*d*₆) δ 11.55 (s, 1H), 8.21 (s, 1H), 7.73 (t, $J = 5.5$ Hz, 1H), 5.94 (s, 1H), 4.49 (d, $J = 5.2$ Hz, 2H), 4.24–4.14 (m, 1H), 2.65 (q, $J = 7.5$ Hz, 2H), 2.43 (q, $J = 7.5$ Hz, 2H), 2.00–1.75 (m, 4H), 1.19–1.07 (m, 6H), 0.69 (t, $J = 7.3$ Hz, 6H). ¹³C NMR (101 MHz, DMSO-*d*₆) δ 164.11, 155.12, 154.93, 153.20, 150.50, 149.33, 140.93, 121.32, 118.80, 104.84, 59.30, 36.67, 27.34 (2C), 26.02, 25.84, 14.96, 13.46, 10.91 (2C). HRMS (ESI): calcd. for C₂₀H₂₇ClN₆NaO [M + Na]⁺: 425.1833 found: 425.1828.

4-(((2-chloro-9-(pentan-3-yl)-9H-purin-6-yl)amino)methyl)-1-methyl-5,6,7,8-tetrahydroisoquinolin-3(2H)-one (**3b3**). White solid, yield:

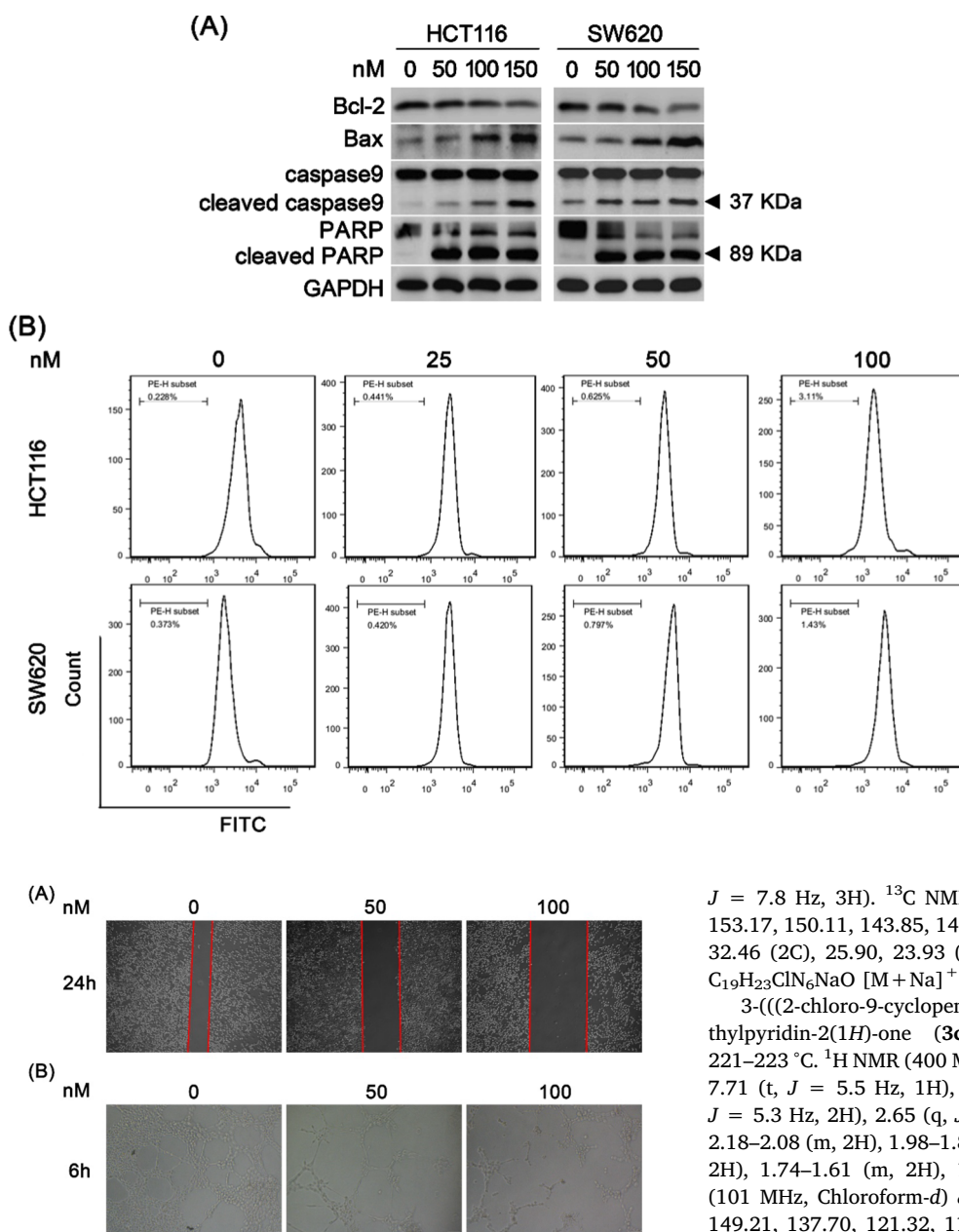


Fig. 8. Effects of SKLB0565 on HUVECs migration and tube formation. (A) Scratches of the cells were created with 200 μ L pipette and images were captured after treatment with indicated concentrations of SKLB0565 for 24 h. (B) Images depicting the formation of capillary-like tubes of HUVECs after treatment with indicated concentrations of SKLB0565 for 6 h.

83.79%, mp 252–254 °C. ^1H NMR (400 MHz, $\text{DMSO-}d_6$) δ 11.54 (s, 1H), 8.20 (s, 1H), 7.80 (t, $J = 5.5$ Hz, 1H), 4.46 (d, $J = 5.2$ Hz, 2H), 4.24–4.15 (m, 1H), 2.89 (s, 2H), 2.37 (s, 2H), 2.11 (s, 3H), 1.97–1.78 (m, 4H), 1.65 (s, 4H), 0.69 (t, $J = 7.3$ Hz, 6H). ^{13}C NMR (101 MHz, Chloroform- d) δ 163.69, 155.04, 154.11, 151.28, 150.45, 141.28, 138.25, 121.05, 118.95, 114.43, 58.78, 36.69, 27.27 (2C), 24.96, 22.44, 22.31, 16.78, 10.49 (2C). HRMS (ESI): calcd. for $\text{C}_{21}\text{H}_{27}\text{ClN}_6\text{NaO}$ $[\text{M} + \text{Na}]^+$: 437.1833 found: 437.1828.

3-(((2-chloro-9-cyclopentyl-9H-purin-6-yl)amino)methyl)-4-ethyl-6-methylpyridin-2(1H)-one (**3c1**). White solid, yield: 82.52%, mp 191–193 °C. ^1H NMR (400 MHz, $\text{DMSO-}d_6$) δ 11.55 (s, 1H), 8.21 (s, 1H), 7.71 (t, $J = 5.5$ Hz, 1H), 5.92 (s, 1H), 4.86–4.69 (m, 1H), 4.49 (d, $J = 4.3$ Hz, 2H), 2.62 (q, $J = 7.3$ Hz, 2H), 2.20–2.05 (m, 5H), 1.99–1.89 (m, 2H), 1.88–1.80 (m, 2H), 1.77–1.62 (m, 2H), 1.11 (t,

Fig. 7. Effects of SKLB0565 on the mitochondrial membrane potential. (A) After treatment with indicated concentrations of SKLB0565 for 48 h, the cells were harvested and lysed for detection of some apoptosis-related proteins. (B) The cells were treated with SKLB0565 for 48 h and $\Delta\Psi_m$ was analyzed by FCM after Rh123 staining.

$J = 7.8$ Hz, 3H). ^{13}C NMR (101 MHz, $\text{DMSO-}d_6$) δ 164.03, 155.00, 153.17, 150.11, 143.85, 140.33, 121.00, 119.01, 106.36, 55.93, 36.63, 32.46 (2C), 25.90, 23.93 (2C), 18.78, 14.89. HRMS (ESI): calcd. for $\text{C}_{19}\text{H}_{23}\text{ClN}_6\text{NaO}$ $[\text{M} + \text{Na}]^+$: 409.1520 found: 409.1511.

3-(((2-chloro-9-cyclopentyl-9H-purin-6-yl)amino)methyl)-4,6-diethylpyridin-2(1H)-one (**3c2**). White solid, yield: 93.32%, mp 221–223 °C. ^1H NMR (400 MHz, $\text{DMSO-}d_6$) δ 11.56 (s, 1H), 8.21 (s, 1H), 7.71 (t, $J = 5.5$ Hz, 1H), 5.94 (s, 1H), 4.81–4.72 (m, 1H), 4.50 (d, $J = 5.3$ Hz, 2H), 2.65 (q, $J = 7.7$ Hz, 2H), 2.43 (q, $J = 7.5$ Hz, 2H), 2.18–2.08 (m, 2H), 1.98–1.88 (m, $J = 14.4$, 7.5 Hz, 1H), 1.88–1.79 (m, 2H), 1.74–1.61 (m, 2H), 1.13 (t, $J = 6.8$, 6.0 Hz, 6H). ^{13}C NMR (101 MHz, Chloroform- d) δ 165.65, 156.43, 154.96, 154.15, 150.18, 149.21, 137.70, 121.32, 119.03, 106.24, 55.60, 36.56, 32.93, 26.35, 26.21, 23.80, 14.81, 12.69. HRMS (ESI): calcd. for $\text{C}_{20}\text{H}_{25}\text{ClN}_6\text{NaO}$ $[\text{M} + \text{Na}]^+$: 423.1676 found: 423.1676.

4-(((2-chloro-9-cyclopentyl-9H-purin-6-yl)amino)methyl)-1-methyl-5,6,7,8-tetrahydroisoquinolin-3(2H)-one (**3c3**). White solid, yield: 91.96%, mp 178–180 °C. ^1H NMR (400 MHz, $\text{DMSO-}d_6$) δ 11.52 (s, 1H), 8.20 (s, 1H), 7.80 (t, $J = 5.5$ Hz, 1H), 4.80–4.70 (m, 1H), 4.46 (d, $J = 4.3$ Hz, 2H), 2.87 (s, 2H), 2.38 (s, 2H), 2.20–2.11 (m, 2H), 2.10 (s, 3H), 1.97–1.86 (m, 2H), 1.856–1.80 (m, 1H), 1.74–1.66 (m, 2H), 1.64 (s, 4H). ^{13}C NMR (101 MHz, Chloroform- d) δ 163.61, 155.10, 154.11, 151.32, 150.16, 141.17, 137.71, 121.05, 119.10, 114.40, 55.58, 36.73, 32.93 (2C), 27.28, 24.95, 23.81 (2C), 22.44, 22.30, 16.82. HRMS (ESI): calcd. for $\text{C}_{21}\text{H}_{25}\text{ClN}_6\text{NaO}$ $[\text{M} + \text{Na}]^+$: 435.1676 found: 435.1671.

3-(((2-chloro-9-(tetrahydro-2H-pyran-2-yl)-9H-purin-6-yl)amino)methyl)-4-ethyl-6-methylpyridin-2(1H)-one (**3d1**). White solid, yield: 88.43%, mp 204–206 °C. ^1H NMR (400 MHz, $\text{DMSO-}d_6$) δ 11.56 (s, 1H), 8.34 (s, 1H), 7.82 (t, $J = 7.9$ Hz, 1H), 5.92 (d, $J = 1.0$ Hz, 1H), 5.65–5.43 (m, 1H), 4.49 (d, $J = 5.3$ Hz, 2H), 4.02–3.95 (m, 1H), 3.75–3.62 (m, 1H), 2.60 (q, $J = 7.6$ Hz, 1H), 2.25–2.15 (m, 1H), 2.13 (s, 3H), 1.93 (m, 2H), 1.73 (m, 1H), 1.56 (m, 2H), 1.10 (t, $J = 7.6$ Hz, 3H). ^{13}C NMR (101 MHz, Chloroform- d) δ 164.71, 157.03, 154.64, 154.45, 149.00, 143.21, 137.60, 120.94, 118.08, 108.10, 81.50, 68.62,

36.16, 31.80, 26.06, 24.68, 22.56, 18.50, 14.43. HRMS (ESI): calcd. for $C_{19}H_{23}ClN_6NaO_2 [M+Na]^+$: 425.1469 found: 425.1463.

3-(((2-chloro-9-(tetrahydro-2H-pyran-2-yl)-9H-purin-6-yl)amino)methyl)-4,6-diethylpyridin-2(1H)-one (**3d2**). White solid, yield: 85.68%, mp 226–228 °C. 1H NMR (400 MHz, DMSO- d_6) δ 11.57 (s, 1H), 8.34 (s, 1H), 7.84 (t, J = 7.9 Hz, 1H), 5.94 (s, 1H), 5.56 (d, J = 10.8 Hz, 1H), 4.50 (d, J = 5.4 Hz, 2H), 4.02–3.95 (m, 1H), 3.75–3.61 (m, 1H), 2.64 (q, J = 7.6 Hz, 2H), 2.43 (q, J = 7.5 Hz, 2H), 2.26–2.13 (m, 1H), 1.93 (m, 2H), 1.73 (m, 1H), 1.56 (m, 2H), 1.13 (t, J = 7.6 Hz, 6H). ^{13}C NMR (101 MHz, DMSO- d_6) δ 164.08, 155.25, 154.98, 153.71, 149.64, 149.35, 139.91, 121.17, 118.58, 104.85, 81.40, 68.14, 36.69, 30.45, 26.01, 25.84, 24.94, 22.77, 14.92, 13.45. HRMS (ESI): calcd. for $C_{20}H_{25}ClN_6NaO_2 [M+Na]^+$: 439.1626 found: 439.1624.

4-(((2-chloro-9-(tetrahydro-2H-pyran-2-yl)-9H-purin-6-yl)amino)methyl)-1-methyl-5,6,7,8-tetrahydroisoquinolin-3(2H)-one (**3d3**). White solid, yield: 89.02%, mp 175–177 °C. 1H NMR (400 MHz, DMSO- d_6) δ 11.54 (s, 1H), 8.33 (s, 1H), 7.93 (t, J = 7.9 Hz, 1H), 5.55 (d, J = 11.2 Hz, 1H), 4.46 (d, J = 5.2 Hz, 2H), 4.02–3.95 (m, 1H), 3.75–3.57 (m, 1H), 2.85 (s, 2H), 2.37 (s, 2H), 2.18 (td, J = 11.6, 3.9 Hz, 1H), 2.10 (s, 3H), 1.93 (m, 1H), 1.75 (m, 1H), 1.64 (s, 4H), 1.56 (m, J = 4.8, 4.3 Hz, 2H). ^{13}C NMR (101 MHz, Chloroform- d) δ 163.55, 155.06, 154.45, 151.45, 149.20, 141.36, 137.54, 120.81, 118.64, 114.49, 81.45, 77.26, 68.72, 36.74, 32.12, 27.26, 24.90, 22.76, 22.40, 22.26, 16.77. HRMS (ESI): calcd. for $C_{21}H_{25}ClN_6NaO_2 [M+Na]^+$: 451.1626 found: 451.1618.

4.1.4. The representative procedure for the preparation of 3-(((2-methylamino-9-substituted-9H-purin-6-yl)amino)methyl)-pyridin-2(1H)-one derivatives (**4a1–4b4**)

3-(((9-isopropyl-2-(methylamino)-9H-purin-6-yl)amino)methyl)-4,6-dimethyl pyridin-2(1H)-one (**4a1**). A mixture of 3-(((2-chloro-9-isopropyl-9H-purin-6-yl)amino)methyl)-4,6-dimethylpyridin-2(1H)-one (190.00 mg, 0.55 mmol) and aqueous methylamine (30%, 10 mL) was stirred in a sealed 35 mL sealed tube at 110 °C for 5 h. A white solid precipitated during the reaction. After the reaction was completed, the suspension obtained was filtered and washed with water (10 mL) to afford a solid product. The crude product was purified by silica gel column chromatography to afford target compounds as white solid with yield 90.52%, mp 206–208 °C. 1H NMR (400 MHz, DMSO- d_6) δ 11.51 (s, 1H), 7.75 (s, 1H), 6.62 (t, J = 3.8 Hz, 1H), 6.25 (q, J = 5.5 Hz, 1H), 5.85 (s, 1H), 4.53 (dd, J = 13.2, 6.5 Hz, 3H), 2.80 (d, J = 4.8 Hz, 3H), 2.26 (s, 3H), 2.10 (s, 3H), 1.45 (d, J = 6.8 Hz, 6H). ^{13}C NMR (101 MHz, DMSO- d_6) δ 163.95, 160.17, 154.75, 148.71, 145.66, 143.09, 135.55, 123.07, 114.14, 108.01, 49.07, 46.03, 28.82, 22.54 (2C), 19.53, 18.64. HRMS (ESI): calcd. for $C_{17}H_{24}N_7O [M+H]^+$: 342.2042 found: 342.2040.

4-ethyl-3-(((9-isopropyl-2-(methylamino)-9H-purin-6-yl)amino)methyl)-6-methylpyridin-2(1H)-one (**4a2**). White solid, yield: 88.98%, mp 166–168 °C. 1H NMR (400 MHz, DMSO- d_6) δ 11.55 (s, 1H), 7.75 (s, 1H), 6.62 (t, J = 3.8 Hz, 1H), 6.25 (q, J = 5.5 Hz, 1H), 5.90 (s, 1H), 4.53 (p, J = 6.7 Hz, 3H), 2.81 (d, J = 4.7 Hz, 3H), 2.63 (q, J = 7.6 Hz, 2H), 2.12 (s, 3H), 1.45 (d, J = 6.7 Hz, 6H), 1.09 (t, J = 7.5 Hz, 3H). ^{13}C NMR (101 MHz, DMSO- d_6) δ 164.29, 160.16, 154.60, 154.27, 151.18, 143.52, 135.57, 122.30, 114.11, 106.44, 55.37, 46.03, 28.77, 26.08, 22.54 (2C), 18.76, 15.15. HRMS (ESI): calcd. for $C_{18}H_{26}N_7O [M+H]^+$: 356.2199 found: 356.2200.

4,6-diethyl-3-(((9-isopropyl-2-(methylamino)-9H-purin-6-yl)amino)methyl)pyridin-2(1H)-one (**4a3**). White solid, yield: 91.30%, mp 176–178 °C. 1H NMR (400 MHz, DMSO- d_6) δ 11.54 (s, 1H), 7.76 (s, 1H), 6.63 (t, J = 3.8 Hz, 1H), 6.26 (q, J = 5.4 Hz, 1H), 5.91 (s, 1H), 4.53 (p, J = 6.7 Hz, 3H), 2.81 (d, J = 4.8 Hz, 3H), 2.65 (q, J = 7.6 Hz, 2H), 2.42 (q, J = 7.6 Hz, 2H), 1.45 (d, J = 6.8 Hz, 6H), 1.11 (dt, J = 12.7, 7.6 Hz, 6H). ^{13}C NMR (101 MHz, DMSO- d_6) δ 164.38, 160.17, 154.60, 154.40, 151.15, 148.99, 135.56, 122.63, 114.11, 104.94, 46.04, 35.90, 28.76, 26.20, 25.82, 22.52 (2C), 15.18, 13.48. HRMS (ESI): calcd. for

$C_{19}H_{28}N_7O [M+H]^+$: 370.2355 found: 370.2352.

3-(((9-cyclopentyl-2-(methylamino)-9H-purin-6-yl)amino)methyl)-4,6-dimethyl pyridin-2(1H)-one (**4b1**). White solid, yield: 90.12%, mp 184–186 °C. 1H NMR (400 MHz, DMSO- d_6) δ 11.51 (s, 1H), 7.72 (s, 1H), 6.62 (t, J = 3.8 Hz, 1H), 6.24 (q, J = 4.6 Hz, 1H), 5.85 (s, 1H), 4.65 (p, J = 7.5 Hz, 1H), 4.50 (d, J = 5.3 Hz, 2H), 2.80 (d, J = 4.8 Hz, 3H), 2.26 (s, 3H), 2.10 (s, 3H), 2.08–1.61 (m, 8H). ^{13}C NMR (101 MHz, DMSO- d_6) δ 163.96, 160.16, 154.76, 151.52, 148.74, 143.09, 136.17, 123.04, 114.19, 108.02, 55.14, 36.36, 32.29 (2C), 28.82, 24.11 (2C), 19.53, 18.64. HRMS (ESI): calcd. for $C_{19}H_{26}N_7O [M+H]^+$: 368.2199 found: 368.2196.

3-(((9-cyclopentyl-2-(methylamino)-9H-purin-6-yl)amino)methyl)-4-ethyl-6-methylpyridin-2(1H)-one (**4b2**). White solid, yield: 87.82%, mp 156–158 °C. 1H NMR (400 MHz, DMSO- d_6) δ 11.53 (s, 1H), 7.72 (s, 1H), 6.62 (t, J = 3.8 Hz, 1H), 6.25 (q, J = 5.2 Hz, 1H), 5.89 (s, 1H), 4.65 (p, J = 7.4 Hz, 1H), 4.53 (d, J = 5.3 Hz, 2H), 2.80 (d, J = 4.8 Hz, 3H), 2.63 (q, J = 7.6 Hz, 2H), 2.12 (s, 3H), 2.10–1.59 (m, 8H), 1.08 (t, J = 7.5 Hz, 3H). ^{13}C NMR (101 MHz, Chloroform- d) δ 165.76, 160.30, 155.83, 154.69, 151.35, 143.61, 134.70, 121.98, 114.54, 107.82, 55.13, 35.77, 32.63 (2C), 28.86, 26.35, 24.04 (2C), 18.91, 14.73. HRMS (ESI): calcd. for $C_{20}H_{28}N_7O [M+H]^+$: 382.2355 found: 382.2351.

3-(((9-cyclopentyl-2-(methylamino)-9H-purin-6-yl)amino)methyl)-4,6-diethylpyridin-2(1H)-one (**4b3**). White solid, yield: 91.27%, mp 194–196 °C. 1H NMR (400 MHz, DMSO- d_6) δ 11.53 (s, 1H), 7.72 (s, 1H), 6.63 (t, J = 3.8 Hz, 1H), 6.25 (q, J = 4.9 Hz, 1H), 5.91 (s, 1H), 4.64 (p, J = 7.6 Hz, 1H), 4.54 (d, J = 5.3 Hz, 2H), 2.80 (d, J = 4.7 Hz, 3H), 2.65 (q, J = 7.5 Hz, 2H), 2.49 (t, J = 1.9 Hz, 3H), 2.41 (q, J = 7.6 Hz, 2H), 2.17–1.55 (m, 8H), 1.12 (t, J = 7.5 Hz, 3H). ^{13}C NMR (101 MHz, DMSO- d_6) δ 164.36, 160.15, 154.60, 154.39, 151.58, 149.00, 136.20, 122.61, 114.15, 104.93, 55.14, 35.82, 32.29 (2C), 28.77, 26.20, 25.82, 24.10 (2C), 15.19, 13.49. HRMS (ESI): calcd. for $C_{21}H_{30}N_7O [M+H]^+$: 396.2512 found: 396.2509.

4-(((9-cyclopentyl-2-(methylamino)-9H-purin-6-yl)amino)methyl)-1-methyl-5,6,7,8-tetrahydroisoquinolin-3(2H)-one (**4b4**). White solid, yield: 89.16%, mp 150–152 °C. 1H NMR (400 MHz, DMSO- d_6) δ 11.53 (s, 1H), 7.72 (s, 1H), 6.69 (t, J = 3.8 Hz, 1H), 6.25 (q, J = 5.7 Hz, 1H), 4.65 (p, J = 7.4 Hz, 1H), 4.51 (d, J = 5.3 Hz, 2H), 2.89–2.74 (m, 4H), 2.50 (p, J = 1.9 Hz, 8H), 2.10 (s, 3H), 2.00–1.77 (m, 4H), 1.63 (d, J = 0.8 Hz, 3H). ^{13}C NMR (101 MHz, DMSO- d_6) δ 162.42, 160.12, 154.73, 149.41, 140.72, 136.17, 122.29, 114.16, 112.34, 55.15, 35.94, 32.28 (2C), 28.80, 27.15, 24.63, 24.10 (2C), 22.56, 22.42, 16.40. HRMS (ESI): calcd. for $C_{22}H_{30}N_7O [M+H]^+$: 408.2512 found: 408.2513.

4.2. Molecular modelling

The 3D structure of the tubulin was downloaded from the PDB (<http://www.rcsb.org/>, PDB code 402B). The protein was prepared with discovery studio 3.1. Molecule SKLB0565 was built with ChemBio3D and optimized at molecular mechanical level. The structure of colchicine was directly extracted from the crystal structure composed of tubulin and colchicine. Then SKLB0565 was docked to the binding site of tubulin by employing a protein-ligand docking program GOLD5.2. Scoring function GOLDScore was used for exhaustive searching, solid body optimizing, and interaction scoring.

4.3. In vitro tubulin polymerization assay

The effects of different concentrations of SKLB0565 (0.05, 1.25, 6.0, 30 μ M) on tubulin polymerization were performed using a fluorescence-based tubulin polymerization kit (BK011P, Cytoskeleton, USA) according to the manufacturer's protocol. Paclitaxel (3 μ M) and CA-4 (1.25 μ M) served as reference compounds and DMSO served as a vehicle control. When the compounds (5 μ L) in 96-well plate were incubated to 37 °C, the corresponding 50 μ L of tubulin reaction mix which contain 2 mg/mL porcine brain tubulin was added to each well. The increase in fluorescence was immediately monitored by excitation at

355 nm and emission at 460 nm in a multimode reader over a 60 min period at 37 °C.

4.4. Cell lines and cell culture

All the cell lines used in our study were purchased from the American Type Culture Collection (ATCC). Cells were cultured in RPMI-1640 containing 10% fetal serum (FBS) and 1% antibiotics (Penicillin and streptomycin) with 5% CO₂ at 37 °C.

4.5. MTT cell proliferation assay

Cell growth was monitored by absorbance using the MTT (3-(4, 5-dimethyl-2-thiazolyl)-2, 5-diphenyl-2H-tetrazolium bromide) assay [34]. Cells were seeded at the density of 2–5 × 10³ cells per well in 96-well cell plates with 100 µL complete medium containing 10% FBS for 24 h. The cells were incubated with different doses of the test compounds for 24, 48 or 72 h. Then, 20 µL of MTT (5 mg/mL) was added and incubated for another 2.5 h at 37 °C. The formazan was dissolved in 150 µL DMSO and the absorbance value of each well was measured at 570 nm after the crystal of purple formazan was dissolved. The IC₅₀ were calculated using Graphpad Prism 8 software.

4.6. Colony formation assay

Cells were seeded at low density (600–800 cells per well) in standard 6-well plates and exposed to different concentrations of SKLB0565. The medium was refreshed every three days. After treatment for 14 days, the cells were fixed with 4% paraformaldehyde for 5 min, and then stained with 0.5% crystal violet for another 10 min. PBS was used to rinse for 2–3 times at last.

4.7. Cell cycle and apoptosis analysis by FCM

For the cell cycle analysis, after treatment with SKLB0565 for 24 h, the cells were harvested and fixed with 75% cold ethanol for at least 2 h and stained with a solution containing PI for 10 min in the dark. Then the cells were analyzed by FCM. The data were analyzed using the FlowJo software.

For the apoptosis assays, the Annexin V- FITC apoptosis detection kit was used as described previously [35]. Cells treated with SKLB0565 for 48 h were harvested and analyzed by FCM using the apoptosis detection kit according to the manufacturer's instructions. The data were analyzed with FlowJo software.

4.8. Mitochondrial membrane potential ($\Delta\Psi_m$) assay

The $\Delta\Psi_m$ of cancer cells was determined after Rh123 staining as described previous [36]. After incubation with different concentrations of SKLB0565 for 48 h, the cells were collected and incubated with Rh123 (5 µg/mL) in the dark at 37 °C for 30 min. Then the fluorescence emitted from Rh123 was detected by FCM. The data were analyzed using the FlowJo software.

4.9. Morphological analysis after Hoechst staining

Morphological changes associated with apoptosis in SW620 cells were detected by Hoechst 33342 (Sigma, USA) staining as described previously [37]. Cells were seeded at 1 × 10⁵ cell per well in 6-well plates and incubated for 24 h. Then different concentrations of SKLB0565 were added and incubated for another 48 h. Finally, the cells were stained with a solution containing Hoechst 33342 (5 µg/mL) according to the manufacturer's instructions. The stained cells were observed and taken photos under an inverted fluorescence microscopy.

4.10. Immunofluorescence (IF) staining

The microtubule organization was observed after immunofluorescence staining of the cells [25]. After treated with the respective compound for 18 h, the cells were fixed in 4% paraformaldehyde for 5 min, washed with PBS and permeabilized with 0.1% Triton X-100 in PBS for 10 min at room temperature (RT). After incubating with the blocking agent for 45 min at RT, the cells were incubated with anti- β -tubulin monoclonal antibody (10094-1-AP, Proteintech, China) overnight at 4 °C. Then the cells were washed three times by PBS following staining by FITC conjugated secondary antibody and labeling of nuclei by DAPI. The cells were finally visualized using a confocal microscope.

4.11. Protein extraction and western blotting analysis

The cells were harvested and homogenized with RIPA buffer containing cocktail and phosphatase inhibitors for western blot analysis. Equal amounts of proteins were separated by SDS-PAGE gel and transferred onto nitrocellulose (NC) filter membranes. After blocking in 5% dried milk in TBS/T, the membranes were incubated with primary antibodies overnight at 4 °C. After incubation with appropriate horseradish peroxidase (HRP)-conjugated secondary antibodies, the expression of proteins was detected by enhanced chemiluminescence (ECL).

4.12. Wound healing assay

The wound healing assay was conducted as described previously with some modification [38]. HUVEC cells were overspread in 6-well plates. Scratches were made in confluent monolayers using 200 µL pipette tip. Then, the wounds were washed twice with sterile PBS to remove nonadherent cell debris. Serum-free medium containing different concentrations of the SKLB0565 (0, 50, 100 nM) were added to the petri dishes. Images were taken by an OLYMPUS inverted digital camera after 24 h incubation.

4.13. Capillary tube formation assay

EC Matrigel matrix thawed at 4 °C was used to coat each well of a 96-well culture plate and allowed to polymerize for an hour at 37 °C. Then, 50 µL of HUVECs (2 × 10⁴ cells per well) were seeded on matrigel-coated well with increasing concentrations of SKLB0565. HUVECs were incubated for 6 h to allow formation of tube-like structures at 37 °C. The images were taken by an OLYMPUS inverted digital camera.

4.14. Statistical analysis

All quantitative results were expressed as means ± SD in 3 independent experiments. Statistically significant differences were obtained using Student's *t*-test. Differences were considered to be statistically significant with a P value less than 0.05.

Declaration of Competing Interest

The authors declare no conflict of interest about this article.

Acknowledgements

We are grateful for Shuhui Xu and Lihua Zhou of State Key Laboratory of Biotherapy (Sichuan University) for NMR measurements and Professor Lijuan Chen's team of State Key Laboratory of Biotherapy (Sichuan University) for HRMS measurements.

Funding

This work was supported by the National S&T Major Special Project on Major New Drug Innovations of China (2018ZX09201018), the

Sichuan Provincial Science and Technology Program for Key Research and Development, China (No. 2018SZ0007), and the Fundamental Research Funds for the Central Universities, China (2017SCU12046, the Postdoctoral Foundation of Sichuan University).

References

- [1] H.V. Goodson, E.M. Jonasson, Microtubules and microtubule-associated proteins, *Cold Spring Harb. Perspect. Biol.* 10 (6) (2018).
- [2] R. Dixit, S. Petry, The life of a microtubule, *Mol. Biol. Cell* 29 (6) (2018) 689.
- [3] P.T. Conduit, Microtubule organization: a complex solution, *J. Cell. Biol.* 213 (6) (2016) 609–612.
- [4] K.H. Downing, E. Nogales, Tubulin structure: insights into microtubule properties and functions, *Curr. Opin. Struct. Biol.* 8 (6) (1998) 785–791.
- [5] C. Garcin, A. Straube, Microtubules in cell migration, *Essays Biochem.* 63 (5) (2019) 509–520.
- [6] L. Cirillo, M. Gotta, P. Meraldi, The elephant in the room: the role of microtubules in cancer, *Adv. Exp. Med. Biol.* 1002 (2017) 93–124.
- [7] J.J. Field, A. Kanakkathara, J.H. Miller, Microtubule-targeting agents are clinically successful due to both mitotic and interphase impairment of microtubule function, *Bioorg. Med. Chem.* 22 (18) (2014) 5050–5059.
- [8] S. Florian, T.J. Mitchison, Anti-microtubule drugs, *Methods. Mol. Biol.* 1413 (2016) 403–421.
- [9] Y.N. Cao, L.L. Zheng, D. Wang, X.X. Liang, F. Gao, X.L. Zhou, Recent advances in microtubule-stabilizing agents, *Eur. J. Med. Chem.* 143 (2018) 806–828.
- [10] E. Bonfoco, S. Ceccatelli, L. Manzo, P. Nicotera, Colchicine induces apoptosis in cerebellar granule cells, *Exp. Cell. Res.* 218 (1) (1995) 189–200.
- [11] G.R. Pettit, S.B. Singh, E. Hamel, C.M. Lin, D.S. Alberts, D. Garcia-Kendall, Isolation and structure of the strong cell growth and tubulin inhibitor combretastatin A-4, *Experientia* 45 (2) (1989) 209–211.
- [12] S.N.A. Bukhari, G.B. Kumar, H.M. Revankar, H.L. Qin, Development of combretastatins as potent tubulin polymerization inhibitors, *Bioorg. Chem.* 72 (2017) 130–147.
- [13] Y. Lu, C.M. Li, Z. Wang, C.R. Ross 2nd, J. Chen, J.T. Dalton, W. Li, D.D. Miller, Discovery of 4-substituted methoxybenzoyl-aryl-thiazole as novel anticancer agents: synthesis, biological evaluation, and structure-activity relationships, *J. Med. Chem.* 52 (6) (2009) 1701–1711.
- [14] S. Kasibhatla, V. Baichwal, S.X. Cai, B. Roth, I. Skvortsova, S. Skvortsov, P. Lukas, N.M. English, N. Sirisoma, J. Drewe, A. Pervin, B. Tseng, R.O. Carlson, C.M. Pleiman, MPC-6827: a small-molecule inhibitor of microtubule formation that is not a substrate for multidrug resistance pumps, *Cancer Res.* 67 (12) (2007) 5865–5871.
- [15] A. Gangjee, Y. Zhao, S. Raghavan, C.C. Rohena, S.L. Mooberry, E. Hamel, Structure-activity relationship and in vitro and in vivo evaluation of the potent cytotoxic anti-microtubule agent N-(4-methoxyphenyl)-N',2,6-trimethyl-6,7-dihydro-5H-cyclopenta[d]pyrimidin-4-amine chloride and its analogues as antitumor agents, *J. Med. Chem.* 56 (17) (2013) 6829–6844.
- [16] D. Cao, Y. Liu, W. Yan, C. Wang, P. Bai, T. Wang, M. Tang, X. Wang, Z. Yang, B. Ma, L. Ma, L. Lei, F. Wang, B. Xu, Y. Zhou, T. Yang, L. Chen, Design, synthesis, and evaluation of in vitro and in vivo anticancer activity of 4-substituted coumarins: a novel class of potent tubulin polymerization inhibitors, *J. Med. Chem.* 59 (12) (2016) 5721–5739.
- [17] Y.T. Chang, S.M. Wignall, G.R. Rosania, N.S. Gray, S.R. Hanson, A.I. Su, J. Merlie Jr., H.S. Moon, S.B. Sangankar, O. Perez, R. Heald, P.G. Schultz, Synthesis and biological evaluation of myoseverin derivatives: microtubule assembly inhibitors, *J. Med. Chem.* 44 (26) (2001) 4497–4500.
- [18] G. Kremmidiotis, A.F. Leske, T.C. Lavanos, D. Beaumont, J. Gasic, A. Hall, M. O'Callaghan, C.A. Matthews, B. Flynn, BNC105: a novel tubulin polymerization inhibitor that selectively disrupts tumor vasculature and displays single-agent antitumor efficacy, *Mol. Cancer Ther.* 9 (6) (2010) 1562–1573.
- [19] Q. Zhang, X. Hu, G. Wan, J. Wang, L. Li, X. Wu, Z. Liu, L. Yu, Discovery of 3-((9H-purin-6-yl)amino)methyl)-4,6-dimethylpyridin-2(1H)-one derivatives as novel tubulin polymerization inhibitors for treatment of cancer, *Eur. J. Med. Chem.* 184 (2019) 111728.
- [20] K.W. Kuntz, J.E. Campbell, H. Keilhack, R.M. Pollock, S.K. Knutson, M. Porter-Scott, V.M. Richon, C.J. Sneeringer, T.J. Wigle, C.J. Allain, C.R. Majer, M.P. Moyer, R.A. Copeland, R. Chesworth, The importance of being Me: magic methyls, methyltransferase inhibitors, and the discovery of tazemetostat, *J. Med. Chem.* 59 (4) (2016) 1556–1564.
- [21] S.K. Verma, X. Tian, L.V. LaFrance, C. Duquenne, D.P. Suarez, K.A. Newlander, S.P. Romeril, J.L. Burgess, S.W. Grant, J.A. Brackley, A.P. Graves, D.A. Scherzer, A. Shu, C. Thompson, H.M. Ott, G.S. Aller, C.A. Machutta, E. Diaz, Y. Jiang, N.W. Johnson, S.D. Knight, R.G. Kruger, M.T. McCabe, D. Dhanak, P.J. Tummino, C.L. Creasy, W.H. Miller, Identification of Potent, Selective, Cell-Active Inhibitors of the Histone Lysine Methyltransferase EZH2, *ACS Med. Chem. Lett.* 3 (12) (2012) 1091–1096.
- [22] M.A. Jordan, L. Wilson, Microtubules as a target for anticancer drugs, *Nat. Rev. Cancer* 4 (4) (2004) 253–265.
- [23] C. Dumontet, M.A. Jordan, Microtubule-binding agents: a dynamic field of cancer therapeutics, *Nat. Rev. Drug. Discov.* 9 (10) (2010) 790–803.
- [24] A. Jordan, J.A. Hadfield, N.J. Lawrence, A.T. McGown, Tubulin as a target for anticancer drugs: agents which interact with the mitotic spindle, *Med. Res. Rev.* 18 (4) (1998) 259–296.
- [25] D. Cao, X. Han, G. Wang, Z. Yang, F. Peng, L. Ma, R. Zhang, H. Ye, M. Tang, W. Wu, K. Lei, J. Wen, J. Chen, J. Qiu, X. Liang, Y. Ran, Y. Sang, M. Xiang, A. Peng, L. Chen, Synthesis and biological evaluation of novel pyranochalcone derivatives as a new class of microtubule stabilizing agents, *Eur. J. Med. Chem.* 62 (2013) 579–589.
- [26] E. Koc, S. Celik-Uzuner, U. Uzuner, R. Cakmak, The detailed comparison of cell death detected by annexin V-PI counterstain using fluorescence microscope, flow cytometry and automated cell counter in mammalian and microalgae cells, *J. Fluoresc.* 28 (6) (2018) 1393–1404.
- [27] R. Shankar, B. Chakravarti, U.S. Singh, M.I. Ansari, S. Deshpande, S.K. Dwivedi, H.K. Bid, R. Konwar, G. Kharkwal, V. Chandra, A. Dwivedi, K. Hajela, Synthesis and biological evaluation of 3,4,6-triaryl-2-pyranones as a potential new class of anti-breast cancer agents, *Bioorg. Med. Chem.* 17 (11) (2009) 3847–3856.
- [28] Q. Hu, D. Wu, W. Chen, Z. Yan, C. Yan, T. He, Q. Liang, Y. Shi, Molecular determinants of caspase-9 activation by the Apaf-1 apoptosome, *Proc. Natl. Acad. Sci. USA* 111 (46) (2014) 16254–16261.
- [29] K. Sinha, J. Das, P.B. Pal, P.C. Sil, Oxidative stress: the mitochondria-dependent and mitochondria-independent pathways of apoptosis, *Arch. Toxicol.* 87 (7) (2013) 1157–1180.
- [30] A. Kamal, T.S. Reddy, M.V. Vishnuvardhan, V.D. Nimbarte, A.V. Subba Rao, V. Srinivasulu, N. Shankaraiah, Synthesis of 2-aryl-1,2,4-oxadiazolo-benzimidazoles: tubulin polymerization inhibitors and apoptosis inducing agents, *Bioorg. Med. Chem.* 23 (15) (2015) 4608–4623.
- [31] A.H. Boulares, A.G. Yakovlev, V. Ivanova, B.A. Stoica, G. Wang, S. Iyer, M. Smulson, Role of poly(ADP-ribose) polymerase (PARP) cleavage in apoptosis. Caspase 3-resistant PARP mutant increases rates of apoptosis in transfected cells, *J. Biol. Chem.* 274 (33) (1999) 22932–22940.
- [32] J.M. Adams, S. Cory, The Bcl-2 protein family: arbiters of cell survival, *Science* 281 (5381) (1998) 1322–1326.
- [33] R.P. Mason, D. Zhao, L. Liu, M.L. Trawick, K.G. Pinney, A perspective on vascular disrupting agents that interact with tubulin: preclinical tumor imaging and biological assessment, *Integr. Biol. (Camb)* 3 (4) (2011) 375–387.
- [34] J. Wang, Z. Jiang, L. Xiang, Y. Li, M. Ou, X. Yang, J. Shao, Y. Lu, L. Lin, J. Chen, Y. Dai, L. Jia, Synergism of ursolic acid derivative US597 with 2-deoxy-D-glucose to preferentially induce tumor cell death by dual-targeting of apoptosis and glycolysis, *Sci. Rep.* 4 (2014) 5006.
- [35] T. Ye, Y. Xiong, Y. Yan, Y. Xia, X. Song, L. Liu, D. Li, N. Wang, L. Zhang, Y. Zhu, J. Zeng, Y. Wei, L. Yu, The anthelmintic drug niclosamide induces apoptosis, impairs metastasis and reduces immunosuppressive cells in breast cancer model, *PLoS One* 9 (1) (2014) e85887.
- [36] Y. Xia, Q. Lei, Y. Zhu, T. Ye, N. Wang, G. Li, X. Shi, Y. Liu, B. Shao, T. Yin, L. Zhao, W. Wu, X. Song, Y. Xiong, Y. Wei, L. Yu, SKLB316, a novel small-molecule inhibitor of cell-cycle progression, induces G2/M phase arrest and apoptosis in vitro and inhibits tumor growth in vivo, *Cancer. Lett.* 355 (2) (2014) 297–309.
- [37] Y.N. Liu, J.J. Wang, Y.T. Ji, G.D. Zhao, L.Q. Tang, C.M. Zhang, X.L. Guo, Z.P. Liu, Design, Synthesis, and Biological Evaluation of 1-Methyl-1,4-dihydroindeno[1,2-c]pyrazole Analogues as Potential Anticancer Agents Targeting Tubulin Colchicine Binding Site, *J. Med. Chem.* 59 (11) (2016) 5341–5355.
- [38] W. Li, Y. Yin, W. Shuai, F. Xu, H. Yao, J. Liu, K. Cheng, J. Xu, Z. Zhu, S. Xu, Discovery of novel quinazolines as potential anti-tubulin agents occupying three zones of colchicine domain, *Bioorg. Chem.* 83 (2019) 380–390.